J Mater Sci (2017) 52:3244–3254

Highly thermostable joint of a Cu/Ni–P plating/Sn–0.7Cu solder added with Cu balls

Takuya Kadoguchi[1,2,*], Naoya Take[3], Kimihiro Yamanaka[4], Shijo Nagao[2], and Katsuaki Suganuma[2]

[1] *Electronic Components Production Engineering Division, Toyota Motor Corporation, Toyota, Aichi, Japan*
[2] *The Institute of Scientific and Industrial Research, Osaka University, Ibaraki, Osaka, Japan*
[3] *Power Electronics Development Division, Toyota Motor Corporation, Toyota, Aichi, Japan*
[4] *School of Engineering, Chukyo University, Nagoya, Aichi, Japan*

Received: 16 July 2016
Accepted: 17 November 2016
Published online: 28 November 2016

© Springer Science+Business Media New York 2016

ABSTRACT

Solder joint reliability in power modules is one of the most important issues for hybrid, electric, and fuel cell vehicles; these modules must have highly reliable solder joints, i.e., they must be highly thermostable at temperatures over 175 °C in the future. The soldering surfaces in power modules are often finished with electroless Ni–P plating. Thus, for Cu/Ni–P plating/Sn–0.7Cu joints, it is necessary to suppress Ni diffusion into the solder. Ni diffusion can be suppressed in the presence of a continuous Cu_6Sn_5 intermetallic compound (IMC) layer at a Ni–P plating/solder interface. To form this IMC, we investigated the composite Sn–0.7Cu solder added with Cu balls. It was confirmed that the addition of 2.5 wt% Cu balls formed a continuous $(Cu, Ni)_6Sn_5$ IMC layer between the solder and the Ni–P plating. It is concluded that the IMC layer works well as a Ni diffusion barrier in multiple reflow tests, of which the peak temperature was 330 °C, and in a high-temperature storage test at 200 °C for 1000 h.

Introduction

To counter the issues of increasing CO_2 emissions and diminishing oil resources, automotive manufacturers have developed various environmentally friendly vehicles, including hybrid, electric, and fuel cell vehicles. All of these vehicles are equipped with power control units (PCU), optimized to maximize the performance of the motors or generators. To leave sufficient space for the driver and passengers, however, the power module of the PCU must provide good fuel efficiency and high power density simultaneously [1–3]. Power modules—currently made from Si semiconductors—can achieve the demand of high power density by operating at high temperature up to 175 °C. There is also new trend toward higher operation temperatures with wide band gap semiconductors such as SiC or GaN [4, 5].

The electrode surface finish in power modules is usually electroless Ni–P plating, which is believed to be reliable and actually has a key role of a solder interconnection [6–10]. Figure 1 shows a schematic drawing of possible failure modes in a Cu/electroless Ni–P plating/Sn–0.7Cu joint. At the interface, a

Address correspondence to E-mail: takuya_kadoguchi@mail.toyota.co.jp

DOI 10.1007/s10853-016-0613-1

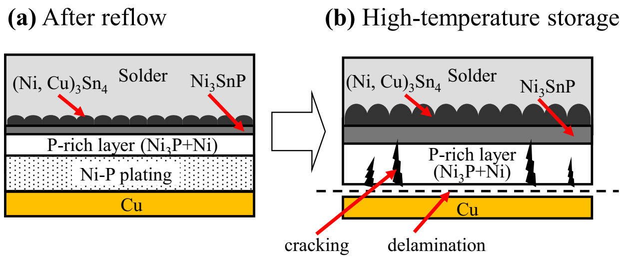

Figure 1 Schematic of device failure mode.

P-rich layer ($Ni_3P + Ni$) and a $(Ni, Cu)_3Sn_4$ intermetallic compound (IMC) are formed [11]. When Ni–P plating is exposed to high temperature or high current density in power modules, Ni easily diffuses into a solder layer. This diffusion decreases the thickness of a Ni–P plating layer and increases the thickness of the $(Ni, Cu)_3Sn_4$ IMC and the P-rich layer. The Ni–P plating layer (P: 9.5 wt%) in this study was amorphous, and compressive stress was applied. Consequently, the volume shrinkage by transformation from an amorphous (Ni–P) layer to a crystal (Ni_3P) one caused cracking and delamination [12, 13]. The lifetime of these modes can be increased by thickening the Ni–P plating [14, 15]. Sn–Cu solder containing more than 3.0 wt% Cu forms a thick Cu_6Sn_5 IMC at the Ni plating surface, which can suppress an excessive interfacial reaction at a Ni–P plating/solder even in a high-temperature storage test [16, 17]. However, increasing the Cu content beyond Sn–0.7Cu eutectic composition sharply raises its liquidus temperature, which requires higher peak reflow temperature. Increasing reflow temperature is not suitable since there are so many peripheral components weak against heat exposure.

Thus, in this study, we proposed a new approach to suppress excessive Ni diffusion by adding tiny Cu balls to Sn–0.7Cu solder. Cu dissolves into the solder much faster than Ni from Ni–P plating does [18]. It is expected that Sn–0.7Cu melts during reflow, and then Cu balls in melting solder partly dissolves and, consequently Cu_6Sn_5 forms on the surface of a Ni–P plating. The addition of Cu balls to Sn–0.7Cu is expected to solve the issue of high-temperature reflow. In the experiment, the peak reflow temperature was 330 °C, which was higher than the liquidus temperature of Sn–3.0Cu, 303 °C [19]. To confirm the thermostability of the soldered joint—electroless Ni–P plating/Sn–0.7Cu solder added with Cu balls—we performed multiple reflows and a high-temperature storage test.

Experimental procedure

Figure 2 shows a schematic drawing of a test sample. The plates to be soldered were made from oxygen-free copper (C1020). A top Cu plate had dimensions of 6.5 mm^2 and 1.0 mm thick, while the base Cu plate had dimensions of 40 × 20 and 3.0 mm thick. These soldering pads of the Cu plates were finished with electrolytic plating of Ni/Au and then with electroless plating of Ni–P. The Ni–P plating was 7–13 μm thick and its P concentration was 9.5 wt%.

The solder was prepared as foils, of which dimensions were 6.5 mm^2 and 0.15 mm thick. Table 1 shows the solder compositions, Cu contents, and sample names. The solder compositions added without Cu balls were Sn–0.7 wt% Cu, Sn–1.6 wt% Cu, and Sn–3.0 wt% Cu corresponding to three types of solders added with Cu balls. The solder composition added with Cu balls was Sn–0.7 wt% Cu. The addition amount of Cu balls were 1.0, 2.0, and 2.5 wt%, respectively. The diameters of the Cu balls were 40–80 μm. The Cu contents of the Sn–0.7Cu samples added with 1.0, 2.0, and 2.5 wt% Cu balls were 1.78, 2.82, and 3.19 wt%, respectively, verified by using inductively coupled plasma mass spectrometry (ICP-MS), which match the intended compositions.

Two Cu plates were joined with the solder foils in a hydrogen reduction reflow furnace. The oxygen concentration in soldering atmosphere was kept less

Figure 2 Schematic of test sample.

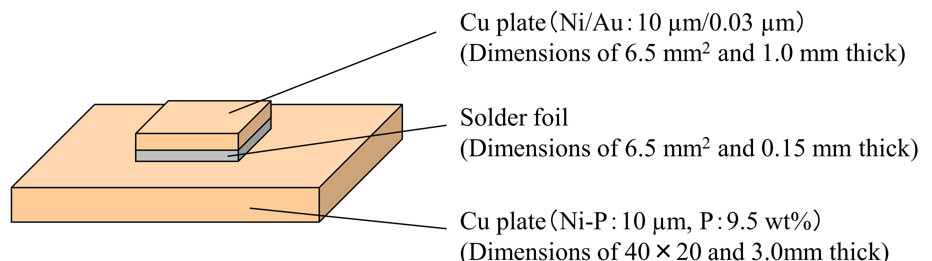

Table 1 Solder composition, Cu content, and sample name

Solder composition	Cu content (by ICP-MS)	Sample name
Sn–0.7 wt% Cu	0.71 wt%	0.7Cu
Sn–1.6 wt% Cu	1.62 wt%	1.6Cu
Sn–3.0 wt% Cu	3.01 wt%	3.0Cu
Sn–0.7 wt% Cu + 1.0 wt% Cu balls	1.72 wt%	0.7Cu + 1.0Cu balls
Sn–0.7 wt% Cu + 2.0 wt% Cu balls	2.82 wt%	0.7Cu + 2.0Cu balls
Sn–0.7 wt% Cu + 2.5 wt% Cu balls	3.19 wt%	0.7Cu + 2.5Cu balls

than 100 ppm. Soldering time beyond 230 °C was over 200 s, and the peak temperature was 330 °C, which is higher than the liquidus temperature of Sn–3.0Cu, 303 °C. Because power modules are often fabricated with multiple soldering steps, the test samples were reflowed by three times. In addition, some of test samples after one reflow were subjected to a high-temperature storage test at 200 °C for 250, 500, and 1000 h.

The cross-sections of the samples were polished and were observed by using a scanning electron microscope (SEM). The IMC phase and composition

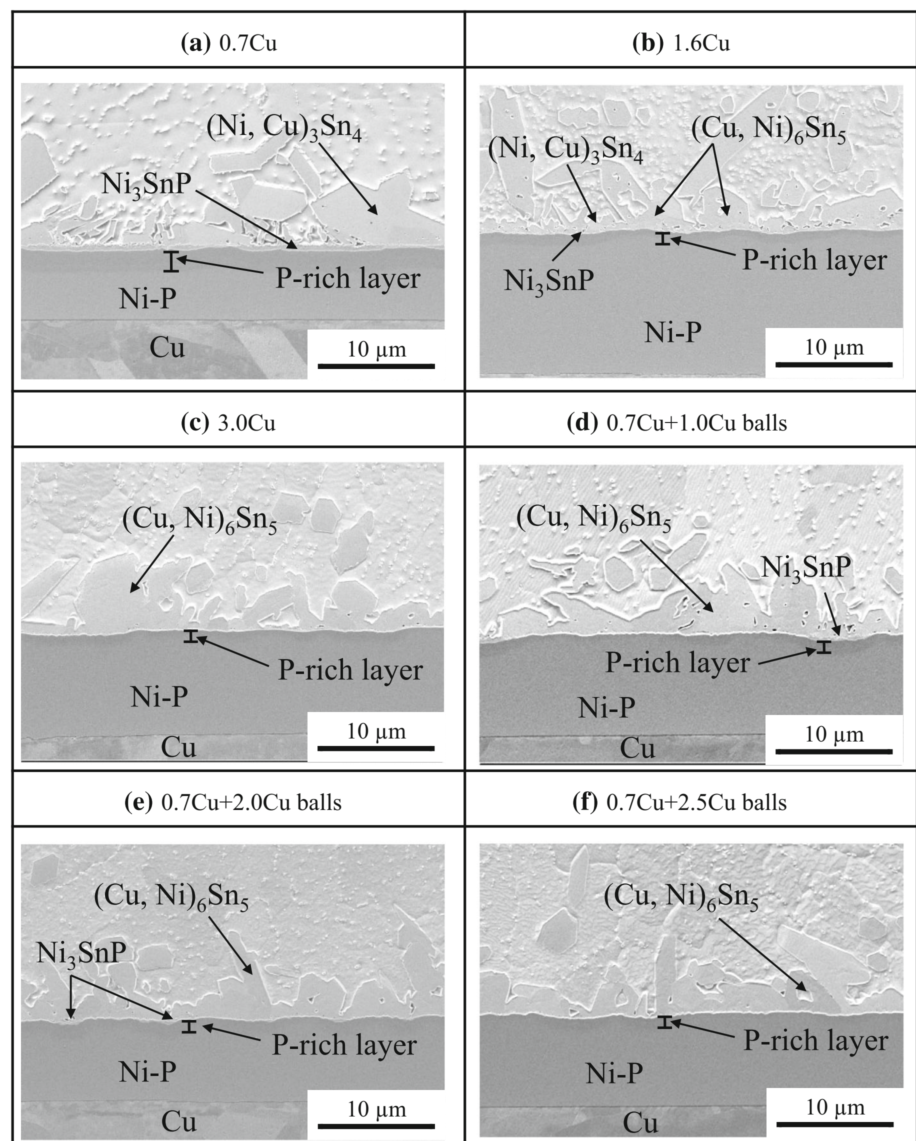

Figure 3 SEM images of Ni–P plating interface after reflow. **a** 0.7Cu; **b** 1.6Cu; **c** 3.0Cu; **d** 0.7Cu + 1.0Cu balls; **e** 0.7Cu + 2.0Cu balls; and **f** 0.7Cu + 2.5Cu balls.

of the joint interface were analyzed by energy-dispersive X-ray spectroscopy (EDX) and X-ray diffraction (XRD). The dissolution speed of the Ni–P plating was also measured in the test samples with SEM. Ni–P plating dissolution thickness, Δi, is defined as follows:

$$\Delta i = d_0 - d_i,$$

where d_0 is the original thickness of the Ni–P plating and d_i is the average thickness of the Ni–P plating after reflow or 200 °C storage test. The thickness of the Ni–P plating was measured at ten locations per sample.

Results and discussion

Soldering interface after one reflow

Figure 3 shows the SEM images of the Ni–P plating interface after reflow. The IMC compositions were analyzed using EDX. The IMC compositions of

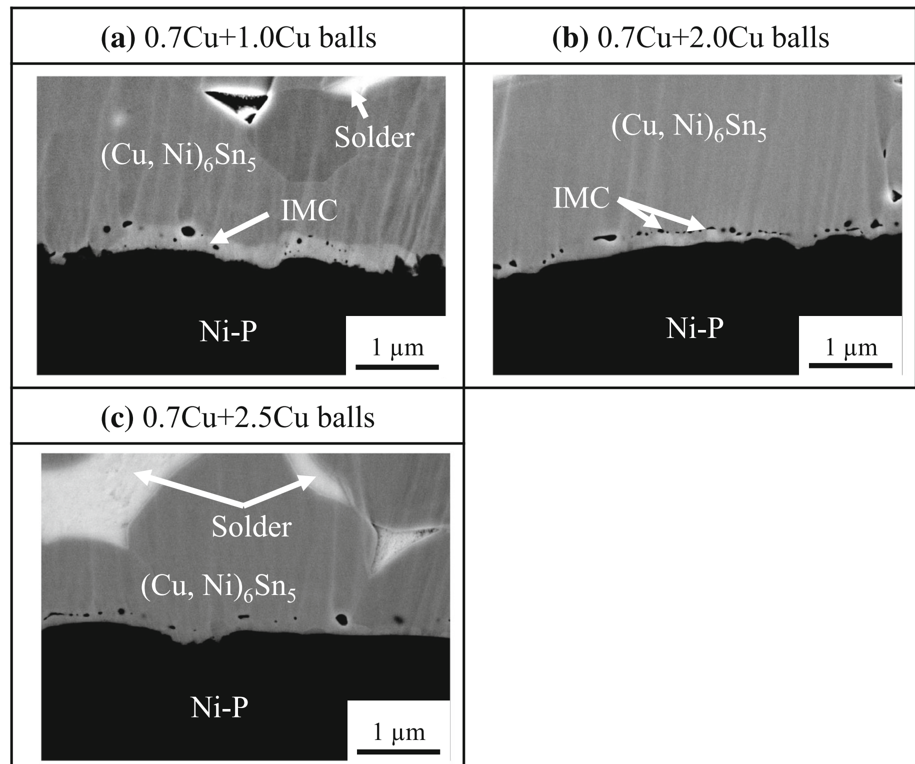

Figure 4 SEM images of Ni–P plating interface after reflow. **a** 0.7Cu + 1.0Cu balls; **b** 0.7Cu + 2.0Cu balls; and **c** 0.7Cu + 2.5Cu balls.

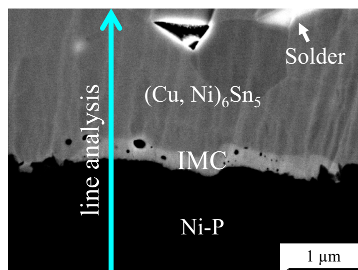

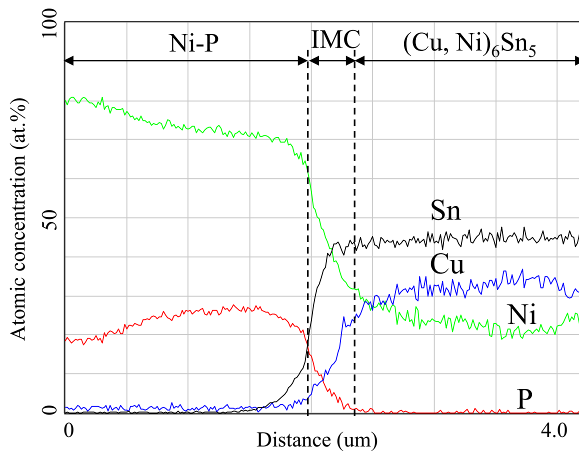

Figure 5 EDX line analysis of 0.7Cu + 1.0Cu balls IMC after reflow.

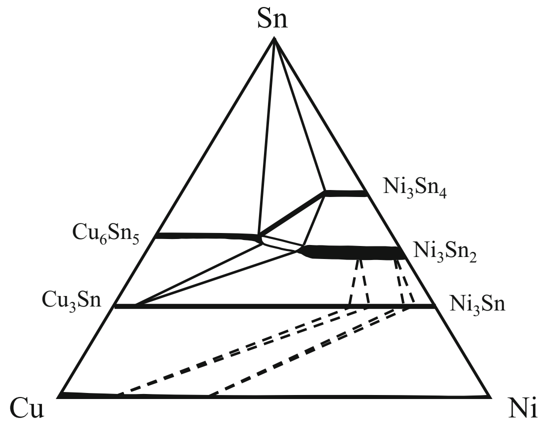

Figure 6 Cu–Ni–Sn isotherm *phase diagram* at 240 °C based on the previous works [23, 24].

(a) 0.7Cu were 37.2 at.% Ni–7.4 at.% Cu–55.4 at.% Sn and 63.6 at.% Ni–17.3 at.% Sn–19.1 at.% P, suggesting the compounds appeared to be (Ni, $Cu)_3Sn_4$ and Ni_3SnP IMC, respectively. These IMCs formed because of interfacial reaction between the Sn–0.7Cu and Ni–P plating during solder melting [20]. The IMCs of (b) 1.6Cu appeared to be Ni_3SnP and a mixture of (Ni, $Cu)_3Sn_4$ and (Cu, $Ni)_6Sn_5$. The IMC of

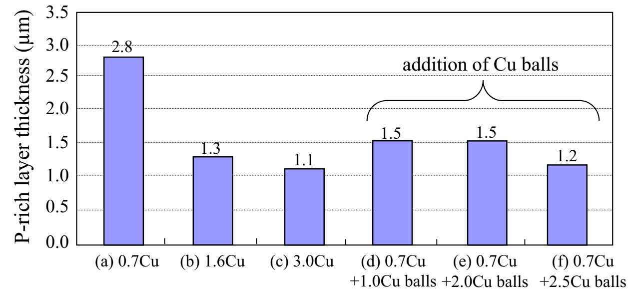

Figure 9 Thickness of P-rich layer after reflow.

(c) 3.0Cu appeared to be (Cu, $Ni)_6Sn_5$. The slow dissolution speed of Ni into the molten solder formed the (Cu, $Ni)_6Sn_5$ IMC [21]. The reaction of (b) 1.6Cu is a transition stage between (a) 0.7Cu and (c) 3.0Cu. The IMCs of (d, e) 0.7Cu + 1.0 and 2.0Cu balls appeared to be (Cu, $Ni)_6Sn_5$ and Ni_3SnP. The IMC of (f) 0.7Cu + 2.5Cu balls appeared to be (Cu, $Ni)_6Sn_5$. The (Cu, $Ni)_6Sn_5$ IMC formed in both the solders added with Cu balls and with the Cu-rich Sn–Cu solder but added without Cu balls. The Ni_3SnP IMC formed when Cu content of Sn–Cu solder without Cu balls was lower than 1.6 wt%, and the Cu balls' content of Sn–0.7Cu solder was lower than 2.0 wt%.

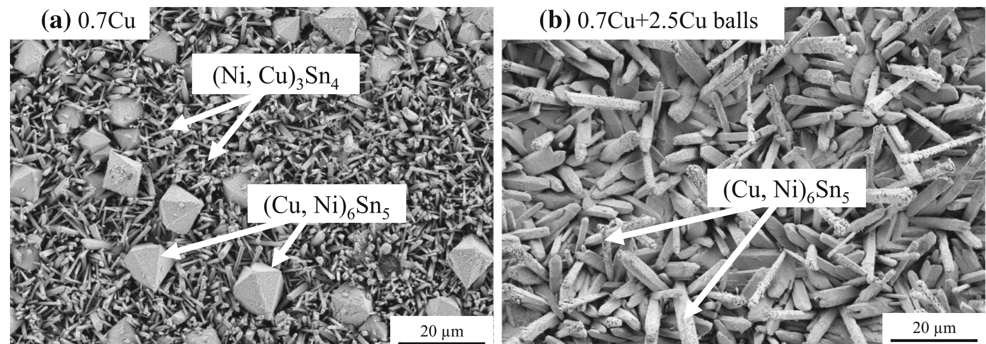

Figure 7 SEM images of IMC at Ni–P plating after reflow. **a** 0.7Cu and **b** 0.7Cu+2.5Cu balls.

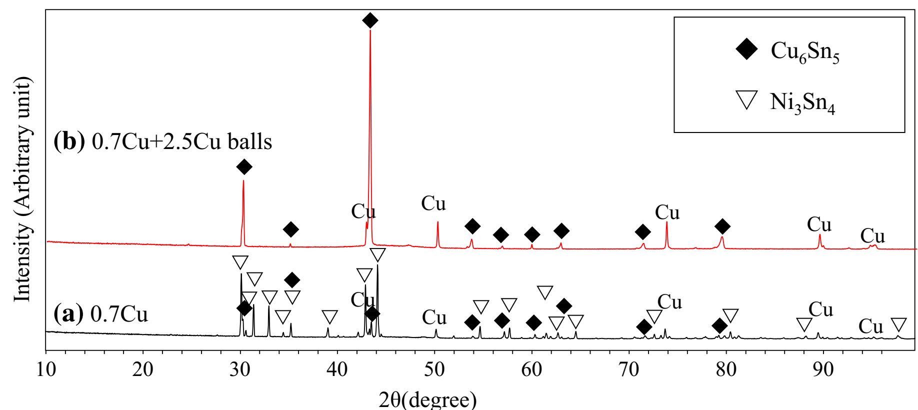

Figure 8 XRD patterns of IMC at Ni–P plating after reflow. **a** 0.7Cu and **b** 0.7Cu + 2.5Cu balls.

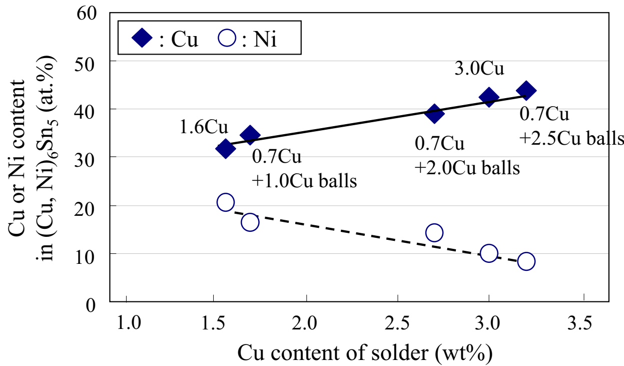

Figure 10 Cu or Ni content in $(Cu, Ni)_6Sn_5$ at Ni–P plating interface.

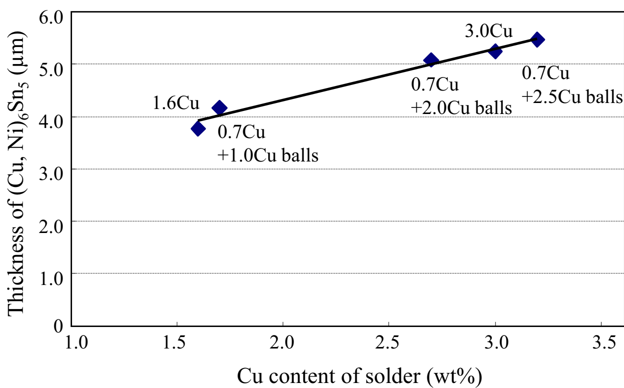

Figure 11 Thickness of $(Cu, Ni)_6Sn_5$ IMC after reflow.

Further, the P-rich layer thickness under the Ni_3SnP IMC slightly grew thicker than the other one in the same sample. The low Cu concentration of Sn–Cu solder was easy to solve the Ni–P plating during solder melting. The behavior of Ni–P depletion-induced Ni_3SnP growth agrees with the previous study [22].

Figure 4 shows the enlarged SEM images of the Ni–P plating interface of the solder added with Cu balls. Back-scattered SEM images were also shown to distinguish each IMC phase between the $(Cu, Ni)_6Sn_5$ and the Ni–P plating in (a, b) 0.7Cu + 1.0 and 2.0Cu balls. These IMCs were 0.1–0.3 μm thick. The IMC of (c) 0.7Cu + 2.5Cu balls consisted of $(Cu, Ni)_6Sn_5$ at the Ni–P plating/solder interface.

Figure 5 shows the EDX line analysis of 0.7Cu + 1.0Cu balls. The Ni contents of the IMC increased, and the Cu contents of the IMC decreased compared with the $(Cu, Ni)_6Sn_5$ IMC. Therefore, this IMC is identified as to be $(Ni, Cu)_3Sn_4$. Such reaction behavior of 0.7Cu + 1.0 and 2.0Cu balls can be understood through the Cu–Ni–Sn isotherm phase diagram because the tie line connects Ni_3Sn_4 and Cu_6Sn_5, as shown in Fig. 6 [23, 24]. However, no tie line connects Ni and Cu_6Sn_5. Thus, the Ni–P/$(Cu, Ni)_6Sn_5$ interface of 0.7Cu + 2.5Cu balls appeared in the current work seems not to be in equilibrium. The $(Cu, Ni)_6Sn_5$ IMC nucleates at the Ni–P plating/solder interface when the molten solder solidifies.

Figure 7 shows the SEM images of the surface IMC at the Ni–P plating interface of (a) 0.7Cu and (b) 0.7Cu + 2.5Cu balls after reflow. To investigate these IMCs in detail, the solder was etched with a mixture of ethanol and hydrochloric acid. The IMCs of (a) 0.7Cu were identified as $(Ni, Cu)_3Sn_4$ and $(Cu, Ni)_6Sn_5$. Though the cross-sectional SEM of Sn–0.7Cu showed the formation of $(Ni, Cu)_3Sn_4$ grains, as shown in Fig. 3a, a broad-surface SEM showed not only $(Ni, Cu)_3Sn_4$ grains but also $(Cu, Ni)_6Sn_5$ grains. This result agrees well with the previous studies [21, 25, 26]. The IMC of (b) 0.7Cu + 2.5Cu balls appeared to be $(Cu, Ni)_6Sn_5$, which agrees with the cross-sectional SEM image shown in Fig. 3f.

Figure 8 compares the XRD results of (a) 0.7Cu and (b) 0.7Cu + 2.5Cu balls. The IMC in (a) 0.7Cu had a mixture of Ni_3Sn_4 and Cu_6Sn_5, while that of 0.7Cu + 2.5Cu balls exhibits a structure based on Cu_6Sn_5.

Figure 9 shows the average thickness of the P-rich layer after reflow. The P-rich layer consists of mixture of Ni_3P and Ni [11]. The P-rich layers of (b) 1.6Cu and (c) 3.0Cu were 1.1–1.3 μm thick which was about a half of that of (a) 0.7Cu. The Cu concentration, which was richer than eutectic Sn–0.7Cu, approached the saturation concentration of Sn–Cu at the reflow peak temperature of 330 °C; this probably suppressed Ni dissolution in the Ni–P plating. The P-rich layers of (d–f) 0.7Cu + 1.0 and 2.0 and 2.5Cu balls were 1.2–1.5 μm thick, and they suppressed the growth of a P-rich layer to about half that of (a) 0.7Cu. The P-rich layer of (f) 0.7Cu + 2.5Cu balls showed a similar thickness as (c) 3.0Cu.

These results clearly show that the addition of Cu balls to Sn–Cu solder suppresses Ni dissolution from Ni–P plating. At the reflow peak temperature of 330 °C, Cu balls dissolved into molten solder much faster than a Ni–P plating. Thus, the faster formation of $(Cu, Ni)_6Sn_5$ IMC on a Ni–P plating suppresses the growth of the P-rich layer as well as high Cu content solder alloys such as 1.6Cu and 3.0Cu.

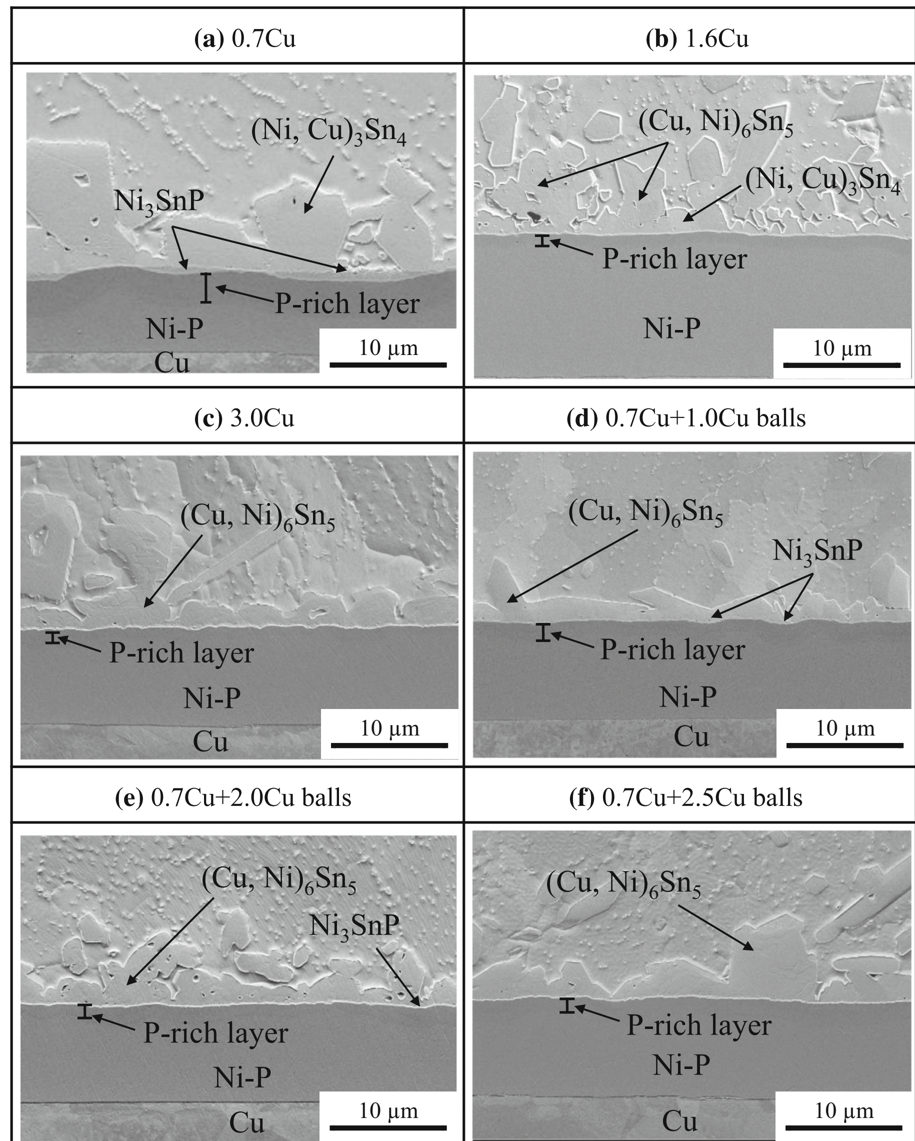

Figure 12 SEM images of Ni–P plating interface after multiple reflows. **a** 0.7Cu; **b** 1.6Cu; **c** 3.0Cu; **d** 0.7Cu + 1.0Cu balls; **e** 0.7Cu + 2.0Cu balls; and **f** 0.7Cu + 2.5Cu balls.

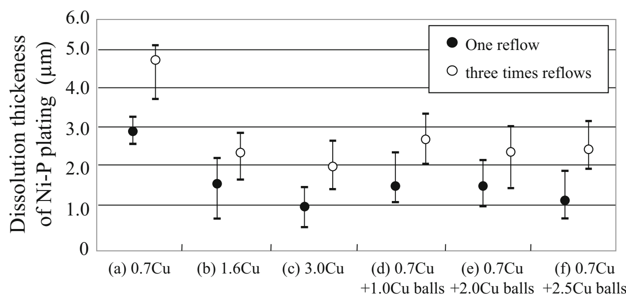

Figure 13 Ni–P plating dissolution in reflow.

Figure 10 shows the Ni or Cu content (at.%) of the (Cu, Ni)$_6$Sn$_5$ IMC as a function of the Cu content (wt%) of the solder. As the Cu content in the solder increased, the Ni content of the (Cu, Ni)$_6$Sn$_5$ IMC decreased, regardless of Cu origin. These results agree with the previous work [27].

Figure 11 shows the average thickness of the (Cu, Ni)$_6$Sn$_5$ IMC as a function of the Cu content (wt%) in the solder. As the Cu content in the solder increased, the thickness of the (Cu, Ni)$_6$Sn$_5$ IMC also increased. The Cu-rich Sn–Cu samples and those added with Cu balls easily formed (Cu, Ni)$_6$Sn$_5$ IMC at a Ni–P plating interface as molten solder solidified. This trend agrees with the previous work [16].

Thus, the addition of Cu balls to Sn–Cu solder formed the (Cu, Ni)$_6$Sn$_5$ IMC resulting in the suppression of excessive Ni dissolution from a Ni–P layer.

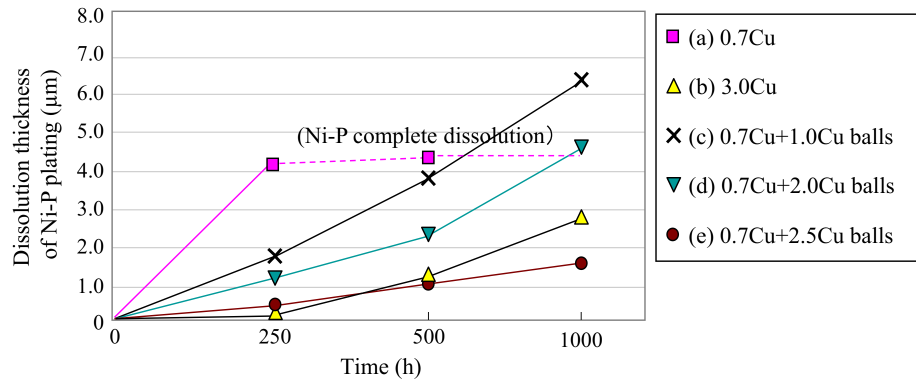

Figure 14 Ni–P plating dissolution as a function of time at 200 °C.

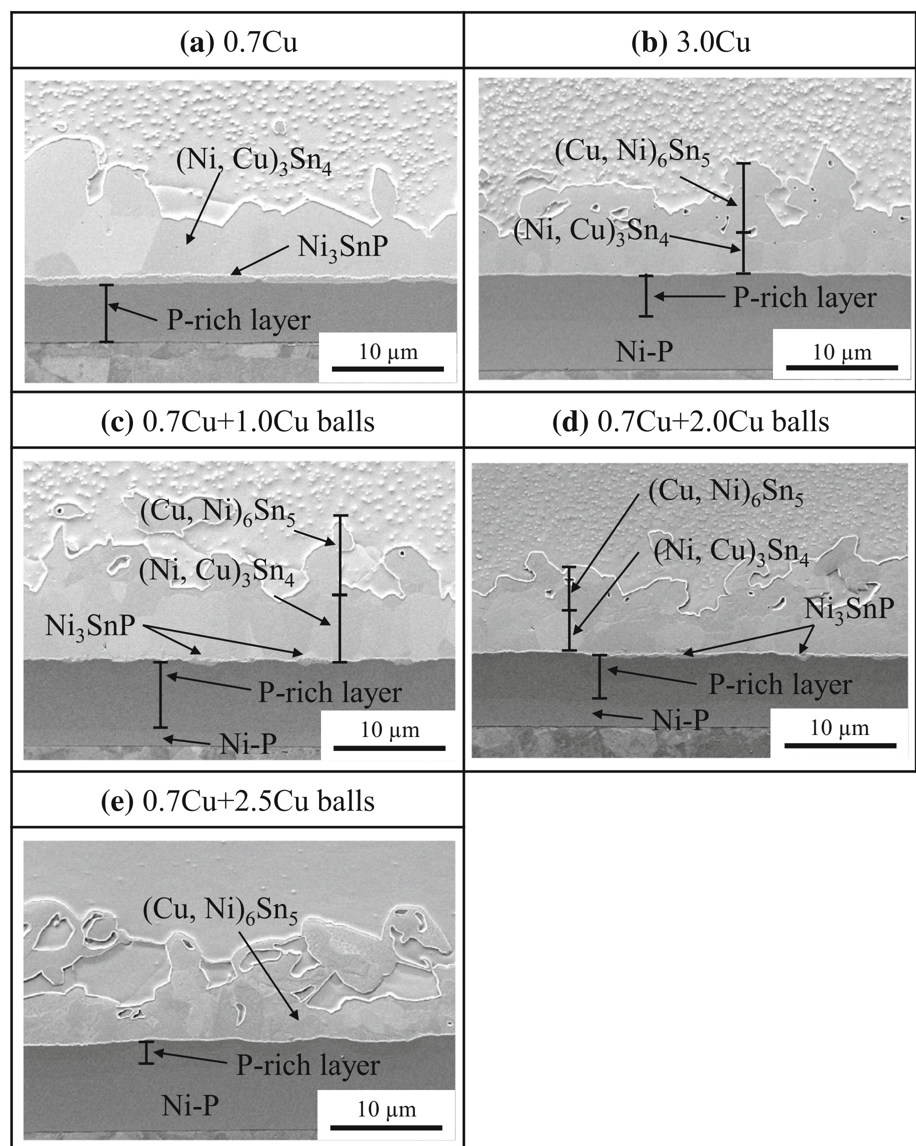

Figure 15 SEM images of Ni–P plating interface at 200 °C. **a** 0.7Cu for 500 h; **b** 3.0Cu for 1000 h; **c** 0.7Cu + 1.0Cu balls for 1000 h; **d** 0.7Cu + 2.0Cu balls for 1000 h; and **e** 0.7Cu + 2.5Cu balls for 1000 h.

Soldering interface after multiple reflows

Figure 12 shows the SEM images of the Ni–P plating/solder interface after three times of reflows. The IMCs of (a) 0.7Cu remained as (Ni, Cu)$_3$Sn$_4$ and Ni$_3$SnP. These layers increased thicknesses from one reflow. Multiple reflows also accelerated the growth of a P-rich layer. The IMCs of (b) 1.6Cu remained as (Ni, Cu)$_3$Sn$_4$ and (Cu, Ni)$_6$Sn$_5$, and the IMC of (c) 3.0Cu remained as (Cu, Ni)$_6$Sn$_5$ after multiple reflows. The IMC of (d–f) 0.7Cu + 1.0 and 2.0 and 2.5Cu balls remained as (Cu, Ni)$_6$Sn$_5$ after multiple reflows.

After multiple reflows, the P-rich layer grew beyond its thickness after one reflow, as shown in Fig. 3. It is interesting to note that the (Ni, Cu)$_3$Sn$_4$ IMC hardly grew except for (a) 0.7Cu. A rapid formation of Cu-based IMC at a Ni–P/solder interface again prevents the growth of the (Ni, Cu)$_3$Sn$_4$ IMC in multiple reflows.

Figure 13 shows the Ni–P plating dissolution after one and three times of reflows. The Ni–P plating dissolution thickness of (a) 0.7Cu was about 4.7 μm, while multiple reflows accelerated Ni dissolution from a Ni–P plating. Ni–P plating dissolution thicknesses of (b) 1.6Cu and (c) 3.0Cu were 2.0–2.3 μm, which was a half of (a) 0.7Cu. Thus, a (Cu, Ni)$_6$Sn$_5$ IMC layer worked well as a Ni dissolution barrier in multiple reflows. The thickness of Ni–P plating dissolution of (d–f) 0.7Cu + 1.0 and 2.0 and 2.5Cu balls was 2.4–2.8 μm thick, which was half of (a) 0.7Cu.

Soldering interface after a high-temperature storage test at 200 °C

Figure 14 shows the Ni–P plating dissolution thickness in a high-temperature storage test at 200 °C. Increasing the amount of Cu balls or Cu content in the solder suppressed the dissipation of the Ni–P plating. After 1000 h, the Ni–P plating dissolution thickness of (e) 0.7Cu + 2.5Cu balls was about 1.8 μm, about one third that of the (c) 0.7Cu + 1.0Cu balls.

Figure 15 shows the SEM images of the Ni–P plating/solder interface at 200 °C. The Ni–P plating layer of (a) 0.7Cu completely consumed and changed into a P-rich layer with the Ni$_3$SnP IMC for 500 h. Increasing the amount of Cu balls or Cu content effectively suppressed the growth of a P-rich layer. However, in (b) 3.0Cu and (c, d) 0.7Cu + 1.0 and 2.0Cu balls, the (Ni, Cu)$_3$Sn$_4$ IMC continuously increased thickness between a (Cu, Ni)$_6$Sn$_5$ IMC and a P-rich layer. The thickness of Ni$_3$SnP did not almost grow thicker than that after reflow. It is reported that the Ni$_3$SnP IMC grows thicker resulting from the reaction between Ni$_3$P and Sn after Ni–P plating depletion. In (c, d) 0.7Cu + 1.0 and 2.0 Cu balls, the Ni–P plating remained after 1000 h. Thus, this result agrees with the previous study [22]. The IMC of (e) 0.7Cu + 2.5Cu balls appeared to be only (Cu, Ni)$_6$Sn$_5$.

Figure 16 shows the EDX line analysis of Sn–0.7Cu + 2.5Cu balls at 200 °C for 1000 h, revealing

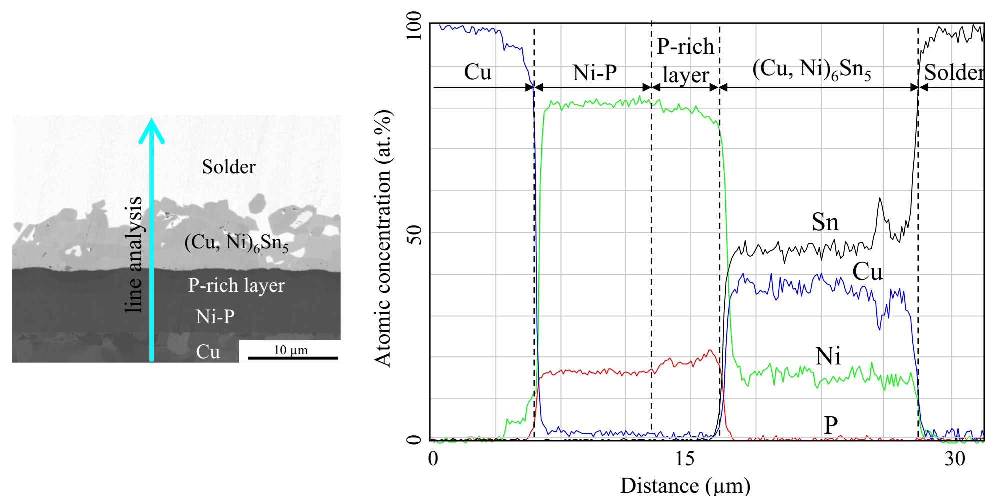

Figure 16 EDX line analysis of Ni–P plating/Sn–0.7Cu + 2.5Cu balls at 200 °C for 1000 h.

that a $(Ni, Cu)_3Sn_4$ IMC did not form between a $(Cu, Ni)_6Sn_5$ IMC layer and a P-rich layer. Yoon et al. reported that in Sn–0.7Cu/Ni plating, $(Ni, Cu)_3Sn_4$ and $(Cu, Ni)_6Sn_5$ IMCs grew at 170 °C for more than 50 days [28]. In this study, a thin $(Ni, Cu)_3Sn_4$ IMC formed during reflow seems to grow during a storage test. In Sn–0.7Cu + 2.5Cu balls, a $(Ni, Cu)_3Sn_4$ IMC did not form after reflow, as shown in Figs. 4 and 8. These results clearly show that a $(Cu, Ni)_6Sn_5$ IMC layer in Sn–0.7Cu + 2.5Cu balls works well as a Ni–P barrier during a high-temperature storage test.

Conclusions

In the present work, a new approach to increase the thermostability of a Cu/Ni–P plating/Sn–0.7Cu solder joint with or without the addition of tiny Cu balls was studied. Multiple reflows and a high-temperature storage test at 200 °C were examined as an acceleration evaluation.

After one reflow, in Sn–0.7Cu + 1.0 and 2.0 and 2.5Cu balls, $(Cu, Ni)_6Sn_5$ IMC formed at a Ni–P plating/solder interface, while, in Sn–0.7Cu, $(Ni, Cu)_3Sn_4$ IMC formed. At the reflow peak temperature of 330 °C, Cu from Cu balls dissolved into a molten solder much faster than Ni from a Ni–P plating. This Cu dissolution effectively formed a $(Cu, Ni)_6Sn_5$ IMC reaction layer at the interface resulting in suppression of the growth of a P-rich layer.

After multiple reflows, a Ni–P plating dissolution thickness of Sn–0.7Cu + 1.0 and 2.0 and 2.5Cu balls was half of that of Sn–0.7Cu. The formation of $(Cu, Ni)_6Sn_5$ IMC at the interface worked as a barrier layer in multiple reflows.

In high-temperature storage test at 200 °C, the addition of Cu balls to Sn–Cu solder suppressed the Ni–P plating dissolution. However, in Sn–0.7Cu + 1.0 and 2.0Cu balls, $(Ni, Cu)_3Sn_4$ IMC continuously formed between a $(Cu, Ni)_6Sn_5$ IMC layer and a P-rich layer, because a thin $(Ni, Cu)_3Sn_4$ IMC discontinuously formed between a $(Cu, Ni)_6Sn_5$ IMC layer and a Ni–P plating layer by reflow. After 1000 h exposure, a Ni–P plating dissolution thickness of Sn–0.7Cu+2.5Cu balls was about one third of that of Sn–0.7Cu + 1.0Cu balls. Thus, Sn–0.7Cu + 2.5Cu balls is concluded as the solder composition to improve the reliability of power modules for harsh environment.

Acknowledgements

The authors would like to thank the students in Chukyo University and colleagues in Toyota Motor Corporation for their helpful discussions.

Compliance with ethical standards

Conflict of interest The authors declare no conflict of interests.

References

[1] Matsubara T, Yaguchi H, Takaoka T, et al (2009) Development of new hybrid system for compact class vehicle. In: Proceedings of JSAE 2009, Japan, p 21

[2] Hamada K (2009) Present status a future prospects for electronics in EVs/HEVs and expectations for wide bandgap semiconductor devices. Mater Sci Forum 600–603:889

[3] Nozawa N, Maekawa T, Yagi E, et al (2010) Development of power control unit for compact class vehicle. In: Proceedings of the 22nd ISPSD 2010, Japan, p 43

[4] Tsuruta K (2011) Prospects of the practical use of SiC power semiconductor devices in automotive applications. Denso Tech Rev 16:90

[5] Hirose S (2014) Power electronics technology for the next generation environmentally-friendly vehicles. In: Proceedings of the 24th microelectronics symposium, JIEP, Japan, p 37 **(Japanese)**

[6] Hirano N, Mamitsu K, Okumura T (2011) Structural development of double-sided cooling power modules. Denso Tech Rev 16:30

[7] Miura S, Ookura Y, Okabe Y et al (2011) Development of power devices for power cards. Denso Tech Rev 16:38

[8] Sakamoto Y (2011) Assembly technologies of double-sided cooling power modules. Denso Tech Rev 16:46

[9] Kadoguchi T, Okumura T, Miyoshi T (2014) Semiconductor module. U.S.Patent, 8,742,556

[10] Kadoguchi T, Iwasaki S, Kawashima T, et al (2014) Semiconductor device and manufacturing method thereof. U.S.Patent, 8,884,411

[11] Hwang CW, Suganuma K, Kiso M et al (2003) Interface microstructure between Ni–P alloy plating and Sn–Ag–(Cu) lead-free solders. J Mater Res 18(11):2540

[12] Baldwin C, Such TE (1968) Plating rates and physical properties of electroless nickel/phosphorus alloy deposits. Trans Inst Metal Finish 46:73

[13] Parker K (1981) Effects of heat treatment on the properties of electroless nickel deposits. Plat Surf Finish 68(12):71

[14] Kadoguchi T, Yamanaka K, Nagao S, et al (2015) Solder electromigration behavior in Cu/electroless Ni–P plating/Sn–Cu based joint system at low current densities. In: Proceeding of the 48th IMAPS, Orlando, p 141

[15] Kadoguchi T, Gotou K, Yamanaka K et al (2015) Electromigration behavior in Cu/Ni–P/Sn–Cu based joint system with low current density. Microelectron Reliab 55:2554

[16] Ikeda O, Serizawa K (2009) Joint reliability of high heat-proof bonding by Sn–Cu solder. In: Proceedings of the 15th Symposium on microjoining and assembly technology in electronics, Japan, p 59 (**Japanese**)

[17] Ho CE, Lin YC, Wang SJ (2013) Sn–Ag–Cu solder reaction with Au/Pd/Ni(P) and Au/Pd(P)/Ni(P) platings. Thin Solid Films 544:551

[18] Bader WG (1969) Dissolution of Au, Ag, Pd, Pt, Cu, and Ni in a molten-tin-lead solder. Weld J Res Suppl 48(12):551

[19] Frear DR et al (1994) The mechanics of solder alloy interconnects. Van Nostrand Reinhold Publishing, New York

[20] Hwang CW, Kim KS, Suganuma K (2003) Interfaces in lead-free soldering. Electron Mater 32(11):1249

[21] Ha JS, Oh TS, Tu KN (2003) Effect of supersaturation of Cu on reaction and intermetallic compound formation between Sn–Cu solder and thin film metallization. J Mater Res 18(9):2109

[22] Ho CE, Hsieh WZ, Yang TH (2015) Depletion and transformation of a submicron Ni(p) film in the early stage of soldering reaction between Sn–Ag–Cu and Au/Pd(P)/Ni(P)/Cu. Electron Mater Lett 11(1):155

[23] Lin CH, Chen SW, Wang CH (2002) Phase equilibria and solidification properties of Sn–Cu–Ni-alloys. Electron Mater 31(9):907

[24] Li CY, Duh JG (2005) Phase equilibria in the Sn rich corner of the Sn–Cu–Ni ternary alloy system at 240 °C. J Mater Res 20:3118

[25] Wang CH, Chen SW (2006) Sn–0.7 wt%Cu/Ni interfacial reaction at 250 °C. Acta Mater 54:247

[26] Ho CE, Yang SC, Kao CR (2007) Interfacial reaction issues for lead-free electronic solders. J Mater Sci 18:155. doi:10.1007/978-0-387-48433-4_10

[27] Ho CE, Tsai RY, Lin YL et al (2002) Effect of Cu concentration on the reactions between Sn–Ag–Cu solders and Ni. Electron Mater 31(6):584

[28] Yoon JW, Kim SW, Jung SB (2005) Interfacial reaction and mechanical properties of eutectic Sn–0.7Cu/Ni BGA solder joints during isothermal long-term aging. J Alloys Compd 391:82